Motional Ground State Cooling Outside the Lamb-Dicke Regime

Y. Yu,* N. R. Hutzler,† J. T. Zhang, L. R. Liu, T. Rosenband, and K.-K. Ni‡

Department of Chemistry and Chemical Biology,
Harvard University, Cambridge, Massachusetts, 02138, USA
Department of Physics, Harvard University, Cambridge, Massachusetts, 02138, USA and
Harvard-MIT Center for Ultracold Atoms, Cambridge, Massachusetts, 02138, USA
(Dated: August 9, 2017)

We report Raman sideband cooling of a single sodium atom to its three-dimensional motional ground state in an optical tweezer. Despite a large Lamb-Dicke parameter, high initial temperature, and large differential light shifts between the excited state and the ground state, we achieve a ground state population of 81(4)% after 100 ms of cooling. In addition, 10 % of initial atom population escapes the trap during cooling. Our technique includes addressing high-order sidebands, , where several motional quanta are removed by a single laser pulse, and fast modulation of the optical tweezer intensity. We demonstrate that Raman sideband cooling to the 3D motional ground state is possible where tight confinement and low initial temperature are difficult to realize.

Trapped neutral atoms, assembled in an array of optical tweezers, are a promising platform to study quantum information and quantum simulations [1–7]. The inherent single-particle detection and control, combined with tunable interactions, allow implementations of neutral-atom-based quantum logic gates [3, 4], novel quantum phases [6], and single-photon switches [8, 9]. Advances in real-time re-arrangement of optical tweezers enable rapid preparation of atoms in large and complex geometries [10, 11]. Quantum motional control of individual atoms [12–16] enable studies of the atomic Hong-Ou-Mandel effect [17], high-fidelity single qubit gates [18], and efficient coupling of single atoms to photonic crystal cavities [19].

Extending optical tweezer arrays to include polar molecules will open up a range of new applications that exploit long-lived molecular internal states and tunable long range interactions [20–22]. Molecules could be assembled from atom pairs in optical tweezers [15], or directly loaded from magneto-optical traps (MOTs) [23–25]. For either approach, preparing the constituent atoms or molecules in the lowest motional quantum state is important to realize long coherence times in quantum applications.

Preparation of single atoms in the motional ground state has been achieved in optical tweezers [13–16] using Raman sideband cooling (RSC) [26–28]. However, RSC in these systems take place in the Lamb-Dicke (LD) regime, where the spread of the initial wavefunctions is much smaller than the wavelength of light used to address them. Systems with a large wavefunction, either due to small mass or high initial temperature, fall outside of the LD regime and undergo strong recoil heating during RSC. Extending RSC beyond the LD regime opens the possibility for ground state cooling of systems such as light atoms and molecules that can be laser-cooled. In this letter we demonstrate cooling of single sodium atoms in optical tweezers, initially outside of the LD regime, to the motional ground state. We achieve a 3D ground state

population of $P_0 = 81(4)\%$ by cooling via high-order sidebands in a carefully optimized cooling sequence. Our approach is general and applicable to other systems.

Our experiment has an overall repetition rate of 2.5 Hz and begins by loading a single sodium atom into optical tweezers from a MOT [29]. The tweezers are created by focussing a 700 nm wavelength laser beam through an NA=0.55 objective to an elliptical waist with radii $\{w_{0,x}, w_{0,y}\} \approx \{0.79, 0.57\}\,\mu$m. For 45 mW of optical power, the trapping frequencies along the three axes are $\{\omega_x, \omega_y, \omega_z\}/2\pi = \{430(4), 590(5), 69(1)\}$ kHz, where z is the weakly confined axial direction, and x and y are the tightly confined radial directions. After each single atom loading attempt, an image is taken with a 1.5 ms exposure time to determine success. During imaging, the atom is cooled via polarization gradient cooling (PGC), which reduces the temperature of the single atom to 70 μK, corresponding to mean motional states along the three trap axes of $\{\bar{n}_x, \bar{n}_y, \bar{n}_z\} = \{3.4(2), 2.5(2), 21(2)\}$, and therefore initial 3D ground state probability of $P_0 = 0.3\%$. The atom is then initialized into the $|F = 2, m_F = -2\rangle$ stretched state via optical pumping (OP). Each experimental cycle ends with a second imaging sequence that measures the hyperfine state of the atom as $|F = 2\rangle$ or $|F = 1\rangle$ [30].

To reduce the temperature of the single atom and achieve high ground state population, we apply Raman sideband cooling [13, 26]. The energy levels, cooling sequence, and Raman beam geometries are shown in Fig. 1. RSC consists of two steps: driving a coherent Raman transition to remove motional quanta, followed by resetting the atom's internal state via OP. These steps are repeated, until the motional ground state is populated with high probability.

Specifically, Raman transitions are driven in Na between the hyperfine states $|2, -2\rangle$ and $|1, -1\rangle$ in the presence of an 8.8 G magnetic field. The external field is orthogonal to the effective magnetic field of the tweezer, to reduce vector light shifts [13, 14]. Subsequently, an
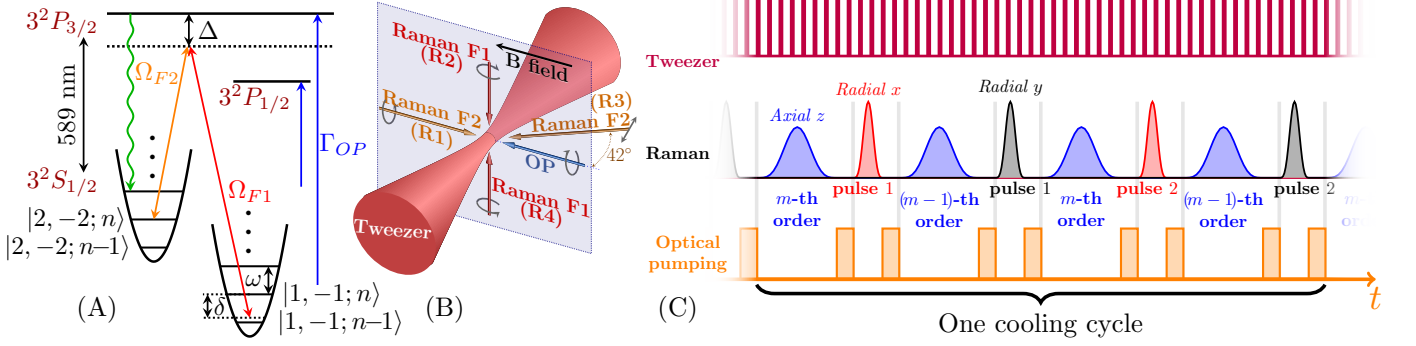
FIG. 1. Single Na atom Raman sideband cooling scheme and sequence. (A) The Raman transitions between $|2, -2; n\rangle$ and $|1, -1; n + \Delta n\rangle$ have a one-photon detuning $\Delta = 25$ GHz below the $3^2S_{1/2}$ to $3^2P_{3/2}$ transition. Two-photon detuning, δ, is defined relative to the $\Delta n = 0$ carrier transition. For optical pumping, we use two σ^- polarized transitions, one to pump the atom state out of $|1, -1\rangle$ via $3^2P_{3/2}$ and one to pump atoms out of $|2, -1\rangle$ via $3^2P_{1/2}$ to minimize heating on the atom in the $|2, -2\rangle$ state. (B) Geometry and polarizations of the Raman and optical pumping beams relative to the optical tweezers and bias magnetic field. Raman beams 1 and 4 address the radial x mode. Raman beams 1 and 2 address the radial y mode. Raman beams 3 and 4 address the axial z mode, which also couples to the radial y mode. (C) Schematic of the cooling pulse sequence. The tweezer is strobed at 3 MHz to reduce light shifts during optical pumping [29]. Each cooling cycle consists of 8 sideband pulses. The four axial pulses address two sideband orders. The two pulses in each radial direction either address $\Delta n = -2$ and $\Delta n = -1$ or have different durations to drive $\Delta n = -1$, when most of the population is below $n = 3$ at the end of the cooling sequence. The Raman cooling and spectroscopy pulses have Blackman envelopes to reduce off-resonant coupling, while the measurement Rabi pulses in Fig. 3(B,C) and 4(B,C) have square envelopes to simplify analysis.

OP pulse, which consists of two frequencies both with σ^--polarization, is applied to bring the atom out of the $F = 1$ manifold and back to $|2, -2\rangle$ via spontaneous emission (Fig. 1A). It is important that the optical pumping step scatter as few photons as possible to minimize recoil heating. Therefore, to optically pump atoms from $|2, -1\rangle$ into $|2, -2\rangle$, we apply light resonant with $3^2P_{1/2}$ [31] because $|2, -2\rangle$ is a dark state to σ^--polarized light [26, 32].

For an atom starting in motional level n_{init}, the probability of recoil during the OP sequence results in a motional-state redistribution is shown in Fig. 2A. The probability is approximately proportional to the square of effective LD parameter $\eta_{\mathrm{eff}}^{\mathrm{OP}} = \sqrt{2n + 1}\eta^{\mathrm{OP}}$ [13], where the optical pumping LD parameter $\eta^{\mathrm{OP}} = z_0 \frac{2\pi}{\lambda}$ is the ratio of the zero-point wavefunction spread $z_0 = \sqrt{\hbar/2m\omega}$ to the reduced wavelength λ. Here, m is the mass of the atom, ω is the trap frequency, and $\hbar$ is the reduced Planck constant. Such heating presents a major challenge for efficient cooling of single Na atoms which feature a low mass (23 amu) and short wavelengths. For our configuration, $\{\eta_x^{\mathrm{OP}}, \eta_y^{\mathrm{OP}}, \eta_z^{\mathrm{OP}}\} = \{0.241(2), 0.206(1), 0.602(5)\}$. A relatively large PGC temperature results in initial $\{\eta_{x,\mathrm{eff}}^{\mathrm{OP}}, \eta_{y,\mathrm{eff}}^{\mathrm{OP}}, \eta_{z,\mathrm{eff}}^{\mathrm{OP}}\} = \{0.67(2), 0.50(1), 4.0(1)\}$. The weak axial direction is far outside of the LD regime ($\eta^2 \ll 1$), and the probability of recoil heating per OP step is large. This creates a large uncertainty on the motional state at the end of a full RSC step, possibly leading to runaway heating.

Fortunately, the large LD parameters also provide opportunities to overcome OP heating. The LD parameter for Raman transitions is defined as $\eta^R \equiv \Delta k z_0$, where the

wave vector is replaced by the wave vector difference Δk between the two beams that drive the Raman transition. The Raman transitions in our configuration have LD pa-
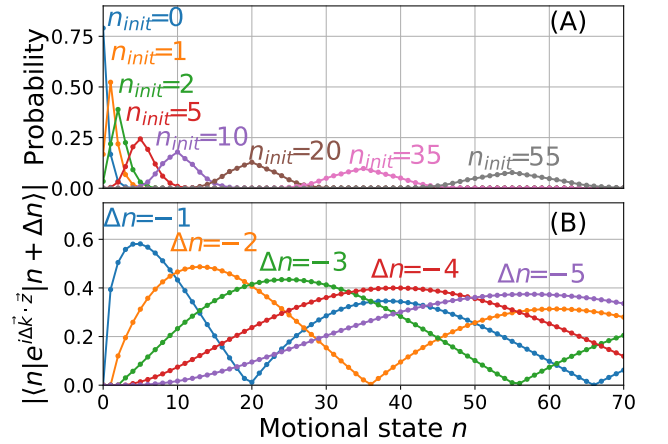

FIG. 2. Optical pumping motional-state redistribution and Raman coupling for large Lamb-Dicke parameters for the axial direction (z). The range plotted covers 95% of the initial thermal distribution. (A) Motional state distribution after one optical pumping cycle for different initial n, n_{init}. Due to photon-recoil and the large Lamb-Dicke parameter, $\eta_z^{OP} = 0.6$, there is a high n changing probability. (B) Matrix elements for Raman transition deviate from $\sqrt{n}$ scaling with multiple minima. During cooling, we utilize the fact that higher motional states couple most effectively to sidebands with large $|\Delta n|$. (k is the difference in wave vector of the Raman beams, r is the coordinate in the axial direction).

rameters of $\{\eta_x^R, \eta_y^R, \eta_z^R\} = \{0.341(2), 0.291(1), 0.40(1)\}$. To offset heating from OP initially, higher-order Raman sidebands ($\Delta n < -1$) can be utilized to remove several motional quanta in a single cooling pulse (see Fig. 2B). Because the coupling strengths of different orders do not reach minima for the same state of motion n, using multiple orders of sidebands avoids accumulations of population near the coupling minima.

Taking the large motional-state changing heating and cooling sources into account, it is not immediately clear that efficient cooling can be achieved. We therefore use a Monte-Carlo simulation to guide our search [33]. In particular, we find that alternating the cooling pulses (Fig. 1C) between two neighboring orders for the axial direction and $\Delta n = -2$ and $\Delta n = -1$ for the radial directions eliminates the accumulation of population in motional states that have zero Raman coupling, which would halt the cooling process. The simulation also indicates that setting the coupling strength of each sideband to drive a Rabi π-pulse corresponding to the maximum matrix element motional state (i.e. the maxima in Fig. 2B) yields efficient cooling, initially. The efficiency of cooling on higher-order sidebands diminishes as the atom approaches the ground state, so the final cycles utilize only the $\Delta n = -1$ sideband while alternating between the three axes.

Guided by the simulation results, we construct our axial cooling sequence by starting at the two highest observed sideband orders ($\Delta n = -8$ and $\Delta n = -7$) and decreasing the orders to the next pair after every 6 to 15 cycles. This process is repeated until we reach $\Delta n = -1$, and most of the population is in the first few excited states. We then switch to cooling only on $\Delta n = -1$ with two different pulse lengths in order to efficiently cool atoms in the few remaining motional states. Radial cooling is performed similarly to the axial cooling with the initial cooling of $\Delta n = -2$ and $\Delta n = -1$ and switching to $\Delta n = -1$ only after 20 to 30 pulses. This sequence gives good initial cooling performance, which can then be used to measure experimental parameters, including the Rabi rates of the Raman beams and optical pumping rates, in order to optimize the sequence further.

There are two additional important challenges in cooling single sodium atoms. First, the high initial temperature populates high motional states, causing the atoms to sample the anharmonicity of the trap away from the center. Anharmonicity may be defined as $A_{i,n} = (E_{i,n+1} - E_{i,n})/h - \omega_i/(2\pi)$ for each trap axis i, and calculated from the quartic term of the optical tweezers via perturbation theory. We find $A_{i,n} = \frac{3n\hbar}{4\pi m d_i^2}$ where $d_i = w_{0,x}, w_{0,y}$ for the radial directions and $d_z = \pi w_{0,x} w_{0,y}/\lambda$. Numerically, $\{A_{x,n}, A_{y,n}, A_{z,n}\} = \{1.1, 2.0, 0.16\}n$ kHz. For mixed states, this broadens high-order sidebands due to the n-dependence of the transitions. In order to mitigate this, we drive the sidebands with a large Rabi frequency

and short pulses to Fourier broaden the spectrum. However, anharmonicity may still shift high-n states out of resonance and prevent effective cooling.

Second, the tweezers cause a large light shift (as large as 300 MHz) in the excited state. We address this by strobing the trapping light at a rate of 3 MHz during the whole cooling sequence, similar to our loading and imaging process [29], while leaving OP on with constant intensity. Due to the large light shift, the OP is effectively off whenever the trap light switches back on. Since the atom is primarily addressed by optical pumping light when the trap light is off, OP remains effective.

Our final cooling results are shown in Fig. 3 and 4. In total, 1000 cooling pulses (total duration 100 ms) are applied along three axes with cooling beginning on the radial second order and axial eighth order. To characterize the single atom thermal state before and after cooling, we perform Raman sideband thermometry [26, 34]. For the more tightly confined (non-degenerate) radial directions, we observe clear $\Delta n = 1$, $\Delta n = -1$, and $\Delta n = -2$ sidebands before RSC, as is shown in Fig. 3A. After cooling, the $\Delta n = -1$ and $\Delta n = -2$ sidebands on both radial axes are strongly reduced. The formula that equates the ratio of $\Delta n = -1$ and $\Delta n = 1$ sideband heights to $\bar{n}/(\bar{n}+1)$ ($\bar{n}$ is the mean motional quantum number of the assumed thermal state) was derived in the LD regime [26]. However, it is also valid outside the LD regime. The resulting $\bar{n}_x = 0.09(3)$ and $\bar{n}_y = 0.05(2)$ correspond to ground-state fractions of $92(2)\%$ and $95(2)\%$, in agreement with fitted values of $89(2)\%$ and $92(2)\%$ from the Rabi flopping curves [34] in Fig. 3B and 3C. The initial temperature of $70\,\mu$K before cooling is obtained from the motional-state decohered Rabi flopping.

For the weak axial direction, cooling is challenging due to the large $\eta_{z,\text{eff}}^{\text{OP}} \approx 4.0(2)$. We observe up to 8th-order Raman cooling sidebands initially, which indicates population in highly-excited motional states. Nevertheless, our cooling sequence works efficiently as all the cooling sidebands are reduced after RSC (Fig. 4). Using the ratio of first-order sideband heights, we obtain $\bar{n}_z = 0.07(3)$, which corresponds to the ground state population of $93(3)\%$, in agreement with a ground state population of $91(2)\%$ extracted from Rabi flopping when $\Delta n = 0$ (Fig. 4B). For the $\Delta n = 1$ sideband Rabi flopping (Fig. 4C), we observe additional decoherence that is more pronounced due to the slower Rabi frequency. The decoherence rate is consistent with magnetic field fluctuations of 1.5 mG measured independently in the lab, which would produce a Zeeman shift of ~ 3 kHz.

Combining the axial and radial cooling results, a single Na atom is in the 3D ground state with a probability of $81(4)\%$ after RSC. We note that there is an additional 5% population loss from imaging and 10% loss from high-lying initial motional states that are not efficiently cooled by RSC, but instead heated out of the trap by off-resonant scattering from the Raman beams.
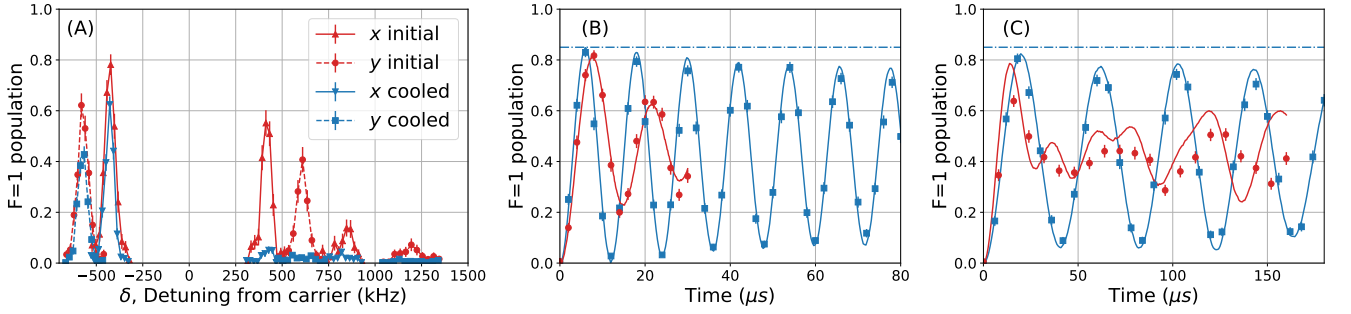
FIG. 3. (A) Left to right: Radial Raman sideband spectrum of $\Delta n_y = 1$, $\Delta n_x = 1$, $\Delta n_x = -1$, $\Delta n_y = -1$, $\Delta n_x = -2$, $\Delta n_y = -2$ before and after Raman sideband cooling. (B,C) Rabi flopping on axis y (B) carrier and (C) $\Delta n_y = 1$ sideband before (red circle) and after (blue square) cooling. Solid lines in (B) and (C) are fits to a Rabi-flopping that includes a thermal distribution of motional states [34] as well as off-resonant scattering from the Raman beams. The curves reach a maximum contrast of 85% (horizontal dashed line) because 5% of atoms are lost from one imaging step to the next, and 10% of atoms are additionally lost during Raman cooling. The blue lines correspond to a 1D ground state probability of 93% after cooling (not including loss) and the red lines correspond to a thermal distribution of 70 μK before cooling.
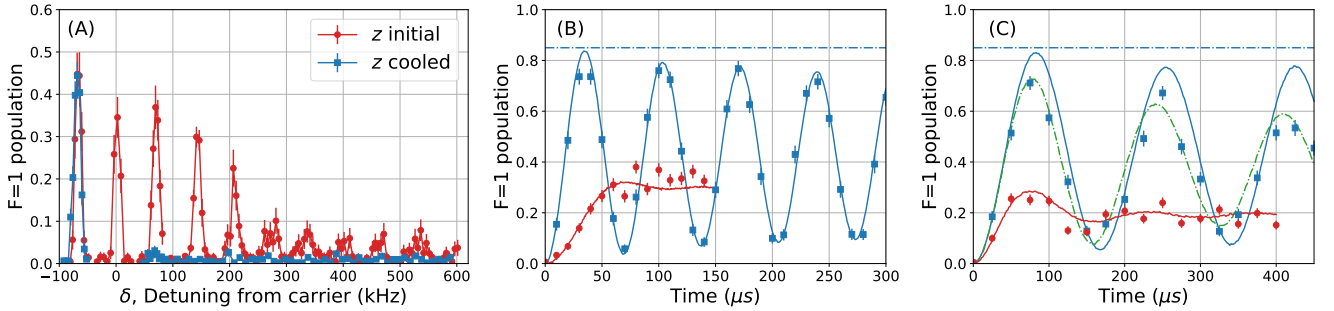

FIG. 4. (A) Left to right: Axial Raman sideband spectrum from $\Delta n_z = 1, 0, -1, \ldots, -8$ before and after Raman sideband cooling. (B,C) Rabi flopping on axial (B) carrier $\Delta n_z = 0$ and (C) $\Delta n_z = 1$ sideband before (red circle) and after (blue square) cooling. Solid blue lines in (B) and (C), similar to Fig. 3B and C, are fits to the Rabi flopping and yield a ground state probability of 92% after cooling (not including the 15% population loss) and the red lines correspond to a thermal distribution of 70 μK before cooling. The green line in (C), includes the additional decoherence due to a fluctuation of the hyperfine splitting of magnitude 3kHz. We see that the decoherence effect is strongest for the post-cooling data on the $\Delta n_z = 1$ sideband where the Rabi frequency is the lowest. The horizontal dashed line shows the overall survival after cooling and imaging.

The cooling efficiency is limited by spontaneous scattering rate (3-15 kHz) from the Raman beams, as well as spectral broadening from magnetic field fluctuations and trap anharmonicity.

We measure a heating rate that corresponds to decreasing of 3D ground state population of single atoms in the tweezers of $\sim 0.9\%$/ms. The rate is consistent with off-resonant scattering of the trapping light [35], and is predominantly in the axial direction where the trapping beam propagates.

We expect to reduce atom losses and enhance the ground state probability after RSC by increasing the detuning of the Raman beams, addressing a wider range of axial trap anharmonicity, implementing better control of the magnetic field, and optimizing imaging. Another improvement could be to implement grey molasses cooling to achieve a lower starting temperature before RSC [36].

We have shown that despite the difficulty in achieving a low optical cooling temperature of low mass sodium atoms, three dimensional cooling with significant ground state population can be achieved by using high-order Raman sidebands in an optimized cooling sequence. These techniques are well-suited for a large variety of systems and open up a route to ground state cooling for other species, including molecules and exotic atoms.

* yichaoyu@g.harvard.edu
† Present address: California Institute of Technology, Division of Physics, Mathematics, and Astronomy. Pasadena, CA, 91125

‡ ni@chemistry.harvard.edu

[1] N. Schlosser, G. Reymond, I. Protsenko, and P. Grangier, Nature **411**, 1024 (2001).

[2] D. S. Weiss, J. Vala, A. V. Thapliyal, S. Myrgren, U. Vazirani, and K. B. Whaley, Phys. Rev. A **70**, 040302 (2004).

[3] L. Isenhower, E. Urban, X. L. Zhang, A. T. Gill, T. Henage, T. A. Johnson, T. G. Walker, and M. Saffman, Phys. Rev. Lett. **104**, 010503 (2010).

[4] T. Wilk, A. Gaëtan, C. Evellin, J. Wolters, Y. Miroshnychenko, P. Grangier, and A. Browaeys, Phys. Rev. Lett. **104**, 010502 (2010).

[5] A. M. Kaufman, B. J. Lester, M. Foss-Feig, M. L. Wall, A. M. Rey, and C. A. Regal, Nature **527**, 208 (2015).

[6] H. Labuhn, D. Barredo, S. Ravets, S. de Léséleuc, T. Macrì, T. Lahaye, and A. Browaeys, Nature **534**, 667 (2015).

[7] S. Murmann, A. Bergschneider, V. M. Klinkhamer, G. Zürn, T. Lompe, and S. Jochim, Phys. Rev. Lett. **114**, 080402 (2015).

[8] B. Dayan, A. S. Parkins, T. Aoki, E. P. Ostby, K. J. Vahala, and H. J. Kimble, Science **319**, 1062 (2008).

[9] T. G. Tiecke, J. D. Thompson, N. P. de Leon, L. R. Liu, V. Vuletić, and M. D. Lukin, Nature **508**, 241 (2014).

[10] D. Barredo, S. de Léséleuc, V. Lienhard, T. Lahaye, and A. Browaeys, Science **354**, 1021 (2016).

[11] M. Endres, H. Bernien, A. Keesling, H. Levine, E. R. Anschuetz, A. Krajenbrink, C. Senko, V. Vuletic, M. Greiner, and M. D. Lukin, Science **354**, 1024 (2016).

[12] X. Li, T. a. Corcovilos, Y. Wang, and D. S. Weiss, Phys. Rev. Lett. **108**, 103001 (2012).

[13] A. M. Kaufman, B. J. Lester, and C. A. Regal, Phys. Rev. X **2**, 041014 (2012).

[14] J. D. Thompson, T. G. Tiecke, A. S. Zibrov, V. Vuletić, and M. D. Lukin, Phys. Rev. Lett. **110**, 133001 (2013).

[15] L. R. Liu, J. T. Zhang, Y. Y. Yu, N. R. Hutzler, Y. Liu, T. Rosenband, and K.-K. Ni, arXiv 1701.03121 (2017).

[16] C. Robens, J. Zopes, W. Alt, S. Brakhane, D. Meschede, and A. Alberti, Phys. Rev. Lett. **118**, 065302 (2017).

[17] A. M. Kaufman, B. J. Lester, C. M. Reynolds, M. L. Wall, M. Foss-Feig, K. R. A. Hazzard, A. M. Rey, and C. A. Regal, Science **345**, 306 (2014).

[18] Y. Wang, A. Kumar, T.-Y. Wu, and D. S. Weiss, Science **352**, 1562 (2016).

[19] J. D. Thompson, T. G. Tiecke, N. P. de Leon, J. Feist, A. V. Akimov, M. Gullans, A. S. Zibrov, V. Vuletic, and M. D. Lukin, Science **340**, 1202 (2013).

[20] D. DeMille, Phys. Rev. Lett. **88**, 67901 (2002).

[21] A. V. Gorshkov, S. R. Manmana, G. Chen, E. Demler, M. D. Lukin, and A. M. Rey, Phys. Rev. A **84**, 033619 (2011).

[22] B. Yan, S. A. Moses, B. Gadway, J. P. Covey, K. R. A. Hazzard, A. M. Rey, D. S. Jin, and J. Ye, Nature **501**, 521 (2013).

[23] J. F. Barry, D. J. McCarron, E. B. Norrgard, M. H. Steinecker, and D. DeMille, Nature **512**, 286 (2014).

[24] S. Truppe, H. J. Williams, M. Hambach, L. Caldwell, N. J. Fitch, E. A. Hinds, B. E. Sauer, and M. R. Tarbutt, (2017), arXiv:1703.00580.

[25] L. Anderegg, B. Augenbraun, E. Chae, B. Hemmerling, N. R. Hutzler, A. Ravi, A. Collopy, J. Ye, W. Ketterle, and J. Doyle, (2017), arXiv:1705.10288.

[26] C. Monroe, D. M. Meekhof, B. E. King, S. R. Jefferts, W. M. Itano, D. J. Wineland, and P. Gould, Phys. Rev. Lett. **75**, 4011 (1995).

[27] A. J. Kerman, V. Vuletić, C. Chin, and S. Chu, Phys. Rev. Lett. **84**, 439 (2000).

[28] D.-J. Han, S. Wolf, S. Oliver, C. McCormick, M. T. DePue, and D. S. Weiss, Phys. Rev. Lett. **85**, 724 (2000).

[29] N. R. Hutzler, L. R. Liu, Y. Yu, and K.-K. Ni, New J. Phys. **19**, 023007 (2017).

[30] The final hyperfine state sensitive detection employs a strong beam that is resonant with the $F = 2$ to $F' = 3$ cycling transition, to heat the $F = 2$ population out of the trap. Therefore, any atoms which survive this heat out procedure are interpreted as having been in the $F = 1$ state.

[31] We find a reduction in the scattering rate by a factor of 130(20), as compared to using an OP resonant with $3P_{3/2}$, from which the $|2, -2>$ state could always scatter a photon via the excited $|F' = 3, m'_F = -3>$ state.

[32] M. Gröbner, P. Weinmann, E. Kirilov, and H.-C. Nägerl, Phys. Rev. A **95**, 033412 (2017).

[33] J. Dalibard, Y. Castin, and K. Mølmer, Phys. Rev. Lett. **68**, 580 (1992).

[34] D. M. Meekhof, C. Monroe, B. E. King, W. M. Itano, and D. J. Wineland, Phys. Rev. Lett. **76**, 1796 (1996).

[35] R. Grimm, M. Weidemüller, and Y. B. Ovchinnikov, Adv. At. Mol. Opt. Phys. **42**, 95 (2000).

[36] G. Colzi, G. Durastante, E. Fava, S. Serafini, G. Lamporesi, and G. Ferrari, Phys. Rev. A **93**, 1 (2016).